JOURNAL OF PROPULSION AND POWER
Vol. 28, No. 5, September–October 2012

Plume Characterization of an Ion-Focusing Hall Thruster

Kunning G. Xu* and Mitchell L. R. Walker†
Georgia Institute of Technology, Atlanta, Georgia 30332

DOI: 10.2514/1.B34433

The T-220HT Hall-effect thruster is modified to include in-channel electrodes and additional magnetic coils to study ion focusing. The goal of this work is to decrease energy losses from ion-wall neutralization and plume divergence to increase the thrust-to-power ratio. In this paper, thrust and plume measurements on xenon are presented. The thruster was tested from 125 to 300 V at 9 A discharge, with the electrodes either floating or biased to 10 or 30 V above anode potential. The mass flow rate was varied from 9.8 to 10.4 mg/s to maintain constant discharge current. The maximum operating chamber pressure was 7.7×10^{-6} Torr-Xe. Performance measurements on xenon show the best overall increase in performance at 150 V discharge and 10 V electrodes with an increase of 7.69 mN of thrust, 4.6 mN/kW thrust-to-power ratio, 123 s I_{SP}, and 5.3% anode efficiency. The plume ion energy distribution function indicates an ion energy increase up to 25 V. The ion number density and propellant efficiency both show increases. The different electrode currents and ion energy distribution functions at 10 V compared with 30 V electrodes suggest different electrode-plasma interaction at the two electrode biases.

Nomenclature

g	=	Earth's gravitational acceleration, 9.81 m/s^2
I_d	=	discharge current, A
I_e	=	electrode current, A
I_{SP}	=	specific impulse, s
$\dot{m}_{tot}$	=	total mass flow rate (includes anode and cathode), mg/s
P_c	=	vacuum chamber background pressure, Torr
P_d	=	discharge power, W
P_e	=	electrode power, W
P_{tot}	=	total power (includes discharge power and electrode power), W
T	=	thrust, N
V_{CG}	=	cathode to ground voltage, V
V_d	=	discharge voltage, V
V_e	=	electrode voltage above the discharge voltage, V
η_A	=	anode efficiency (includes electrode power)

I. Introduction

HALL-effect thrusters (HETs) are one of the prime candidates for use as primary propulsion systems for satellites. They provide a combination of thrust and specific impulse (I_{SP}) that offers advantages for many near-Earth missions. They have been studied in Russia, the United States, and elsewhere. Their performance has been demonstrated in laboratory tests and in orbit. Some satellite missions desire short, high-thrust burns for quick orbit changes. This requires a high thrust-to-power (T/P) ratio. This work looks to reduce loss sources within the thruster as a means to increase T/P ratio, specifically ion losses caused by ion-wall neutralization. A HET typically achieves maximum T/P at low discharge voltage. At low discharge voltages, the ionization rate decreases because of weaker electric fields and a reduction in the energy of the electrons. With a lower ion number density, any ions lost to wall neutralizations greatly reduces the performance of the thruster. Thus a reduction in ion-wall collisions could increase T/P and thruster efficiency. This research attempts to reduce such collisions through the use of electrodes embedded in the discharge channel wall to focus ions.

Ion focusing is performed with the addition of inner and outer wall electrodes inside the discharge channel and a second pair of electromagnets to generate cusp magnetic fields to shield the electrodes. The electrode guides ions with trajectories intersecting the chamber wall towards the centerline of the chamber focusing the ions, which results in an increase in efficiency and T/P. A T-220HT thruster is modified for this work and named the embedded electrode Hall-effect thruster (EEHET). The study of ion focusing dates back to the early 1970 s. Morozov et al. [1]. noted the constant potential along magnetic field lines and the ability to focus the ion beam with proper design of the magnetic field. To a great extend, the history of the HET has been about optimizing the magnetic field. Current thrusters such as the Busek BHT-1000, Aerojet BPT-4000, and the 6 kW Hall thruster at Michigan all generate high T/P levels at low voltages [2–5]. The BHT-1000 has a similar dual electrode design inside the discharge channel. The differences between that thruster and the EEHET are the thin ring electrodes used in the EEHET and the addition of the shielding ring-cusp fields around the electrodes to reduce electron collection.

In this work, performance and plume measurements are taken for the EEHET on xenon. The goal is to determine the effect of the in-channel electrodes on the thruster. The electrodes generate an electric field near the channel surface that should repel ions that come in contact with the field. This should divert ions to a more axial path. This reduces ion-wall neutralization, which increases ion density and decreases the plume divergence angle. Section II discusses the experimental setup. Section III presents the results of thrust and plume measurements. Section IV presents an analysis of the results and discussion of the implications.

II. Experimental Setup

A. Hall Thruster

All of the experiments were performed on a modified Pratt & Whitney T-220HT Hall thruster. Extensive testing has mapped the performance of the base thruster over a power range of 2–22 kW at discharge voltages of 200–600 V [6]. The T-220HT has a mean channel diameter of 188 mm, a channel depth of 65 mm, and a nominal power rating of 10 kW. An Electric Propulsion Laboratory 375 series cathode is located at the 12 o'clock position of the thruster and declined approximately 40 deg to the horizontal to be aligned with the local magnetic field. The cathode orifice is located

Presented at the 47th AIAA/ASME/SAE/ASEE Joint Propulsion Conference and Exhibit, San Diego, July 31–August 3 2011; received 21 August 2011; revision received 15 March 2012; accepted for publication 16 March 2012.

*Graduate Student, High-Power Electric Propulsion Laboratory, Aerospace Engineering, 270 Ferst Dr. NW. Member AIAA.

†Associate Professor, High-Power Electric Propulsion Laboratory, Aerospace Engineering, 270 Ferst Dr. NW. Associate Fellow AIAA.

approximately 1.5 cm downstream from the thruster exit plane. The cathode flow rate is set to a constant 1 mg/s for all cases investigated. The discharge channel of the thruster is made of M26 grade boron nitride. A more detailed description of the T-220HT and its characteristics can be found in [7].

The T-220HT HET discharge supply is a 45 kW Magna-Power TSA800-54 power supply, and all other thruster components are powered with TDK-Lambda 1 or 3.3 kW Genesys power supplies. All electrical connections enter the chamber through separate feedthroughs. The thruster discharge supply is connected to a remote-control filter consisting of a 1.3 Ω resistance and 95 μF capacitor. The filter acts as a low pass filter preventing oscillations in the discharge current over 1.4 kHz from reaching the discharge supply. High-purity (99.9995%) xenon propellant is supplied with MKS 1179A mass flow controllers to the cathode and anode with an uncertainty of ±0.03 and ±0.2 mg/s, respectively. The flow controllers are calibrated by measuring gas pressure and temperature as a function of time in a known control volume.

B. Ion Focusing

Ion focusing is achieved with the application of positively biased electrodes embedded in the inner and outer channel surfaces. The electrode power supply negative is electrical connected to the anode power line and thus biased above anode potential. The resultant electric fields should repel off-axis ions and reduce wall collisions. To reduce electron collection by the positively biased electrodes, cusp-shaped magnetic fields are placed over the electrodes. The cusp fields magnetize electrons moving toward the electrodes, which reduces electron mobility and collected current. The static magnetic fields in the thruster are analyzed with the software MagNet by Infolytica and modified to generate the cusp magnetic fields along specific sections of the channel wall. The resultant cusp field magnetizes 25 eV electrons, resulting in a 2 mm electron gyroradius at a distance 5 mm from the electrode and 0.7 mm gyroradius at a distance 2 mm from the electrodes. Figure 1 shows the final 2-D magnetic field with components and field strengths indicated. The field shape and strength is confirmed with physical Gauss probe measurements to within 5%. Figure 2 shows a schematic of the electrode electrical connections. The discharge voltage, V_d, and electrode voltage, V_e, are measured between their respective power supply leads. The discharge current, I_d, and electrode current, I_e, are measured from the cathode and electrode lines, respectively.

C. Thrust Stand

Thrust is measured with a null-type inverted pendulum thrust stand based on the NASA John H. Glenn Research Center at Lewis Field design by Haag [7]. The null-type stand holds the thruster at a constant position with the use of proportional-, integral-, and derivative-controlled solenoid coils that move a center magnetic rod. A linear variable differential transformer measures the thrust stand position and provides feedback for power amplifiers in the control loop. Thrust is correlated to the amount of current on the null coil required to hold the thrust stand at the zero position. Thrust stand calibration is performed by loading and off-loading a set of known weights over the range of expected thrust. The resultant linear curve of null-coil current versus weight is used as the conversion for thrust measurements. A copper shroud surrounds the stand, and coolant is passed through to maintain thermal equilibrium. Further details of the thrust stand and its operation can be found in [8].

The thrust stand has a measurement noise error of ±0.8 mN. The thruster is shut down every 40–60 min after each firing to recalibrate and determine the zero position. This procedure minimizes thermal drift in the null coil, which reduces uncertainty. The thrust uncertainty is thus primarily due to the measurement noise and is estimated at ±1.5%. T/P, I_{SP}, and anode efficiency error are based on measurement device uncertainly and are all less than ±3%.

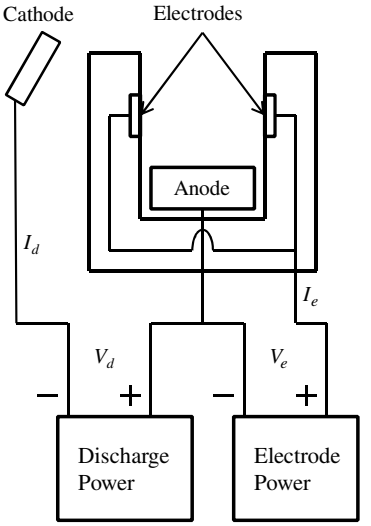

Fig. 2 EEHET electrical schematic.

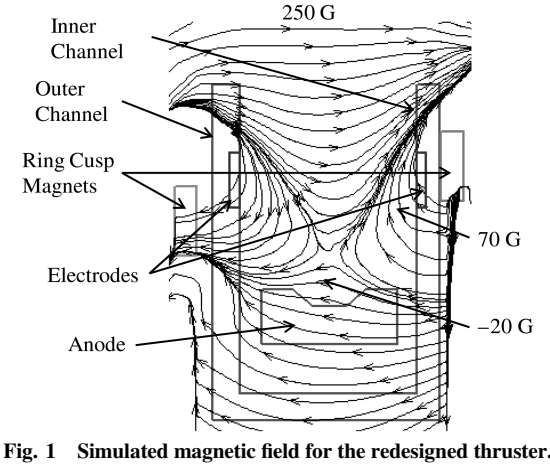

Fig. 1 Simulated magnetic field for the redesigned thruster.

D. Faraday Probe

The Faraday probe is a simple plasma diagnostic used to measure ion current density in the HET plume. Its use has been well documented [8–12]. Figure 3 shows an electrical schematic of the Faraday probe used in this work. The probe is based on the Jet Propulsion Laboratory nude Faraday probe design [9]. It consists of a 2.31-cm-diameter tungsten-coated stainless-steel collection electrode with a stainless-steel guard ring surrounding it. A gap of 0.12 cm exists between the electrode and guard ring between. A Lambda GENH 60-12.5 power supply biases the collector and shield to 20 V below ground. Biasing the collector and guard ring to the same potential reduces edge effects by creating a uniform sheath potential around the collector. Voltage measurements across a 1.417 kΩ, 0.5 W resistor placed in series with the collector line is read by an Agilent 34980A data acquisition unit.

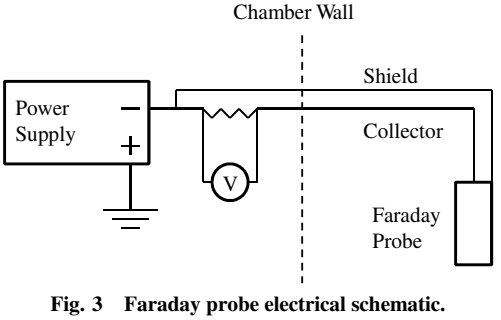

Fig. 3 Faraday probe electrical schematic.

The probe arm is centered over the thruster exit plane. The collector surface is placed 1 m downstream of the thruster exit plane. Sweeps are taken from −100 to +100 deg from thruster centerline in 1 deg increments. Measurements are taken at 80 Hz sample rate for 1 s at each position and averaged to produce the recorded current density at that location. The measurements are taken at a single radial distance. Background pressure effects are not studied, although the operating pressure is always below 7.7×10^{-6}, which minimized the pressure effects on the data. The uncertain in Faraday probe measurements caused by charge-exchange collisions is estimated at ±10% for the beam current and divergence angle through analysis of variance.

E. Retarding Potential Analyzer

A retarding potential analyzer (RPA) measures ion energy per charge with a series of biased grids to selectively filter ions [13,14]. The RPA cannot discriminate between singly- and multiply-charged ions. The RPA acts as a high-pass filter that only allows ions with energy higher than the ion repulsion grid to pass through to the collector. By increasing the voltage on the ion retarding grid, ions with equal or less energy are repelled, and the collected current drops. The negative derivative of the resulting current-voltage data, $-\mathrm{d}I/\mathrm{d}V$, is proportional to the ion energy distribution function [13].

The RPA used in this work consists of four grids and a collector based on the design used in [1]. In order from plasma to collector, they are the floating, electron repulsion, ion repulsion, and electron suppression grids. The floating grid floats to the plasma potential to reduce perturbations caused by the probe presence. The electron repulsion grid is negatively biased with respect to ground to repel plasma electrons, and the ion repulsion grid is positively biased with respect to ground to retard ions. The electron suppression grid is biased negative with respect to ground to repel any secondary electrons emitted from the collector because of ion collisions. The electron repulsion and suppression grids are both biased to −30 V by a pair of GENH 60-12.5 power supplies. The ion repulsion grid is powered by a Keithley 2410 Sourcemeter. The collector current is measured with a Keithley 6487 Picoammeter. Both the sourcemeter and picoammeter are controlled with LabVIEW. RPA data are collected at 10 angles from centerline through the plume: 0, 5, 10, 15, 20, 25, 30, 40, 50, and 60 deg. The uncertainty in the most probable ion potential is estimated as 50% of the half width at half-maximum value of the potential peak [5]. This uncertainty varies depending on discharge voltage and has a maximum value of ±6.5 V.

F. Vacuum Facility

All of the experiments are performed in the vacuum test facility 2 (VTF-2) at Georgia Tech shown in Fig. 4. VTF-2 is a stainless steel chamber 9.2 m long and 4.9 m in diameter. It is pumped to rough vacuum with one 3800 CFM blower and one 495 CFM rotary-vane pump. Ten liquid nitrogen cooled CVI TMI re-entrant cryopumps with a combined pumping speed of 350, 000 l/s on xenon bring the chamber to a base pressure of 5×10^{-9} Torr. A Stirling Cryogenics SPC-8 RL special closed-looped nitrogen liquefaction system supplies liquid nitrogen to the cryopump shrouds. Two ionization gauges, Varian 571 and UHV-24, are mounted on either side of the chamber.

III. Results

The thruster is operated over 125–300 V discharge voltage at a discharge current of 9 ± 0.1 A. The electrodes are operated at three conditions: electrically floating, biased to 10 V above anode potential, and biased to 30 V above anode potential. These three conditions are noted as floating, 10 V_e, and 30 V_e, respectively. Figure 5 shows the current collected by the electrodes. The electrode current is quite different between the two bias levels. Because the electrodes are connected to the anode power line, they share current with the main anode. This means at 30 V_e, when the electrodes draw over 9 A of current, the anode has little to no current. This causes the electrodes to act as the primary anode. Some current recycling occurs between the electrode and anode within the circuit as the discharge power supply current is held at 9 A.

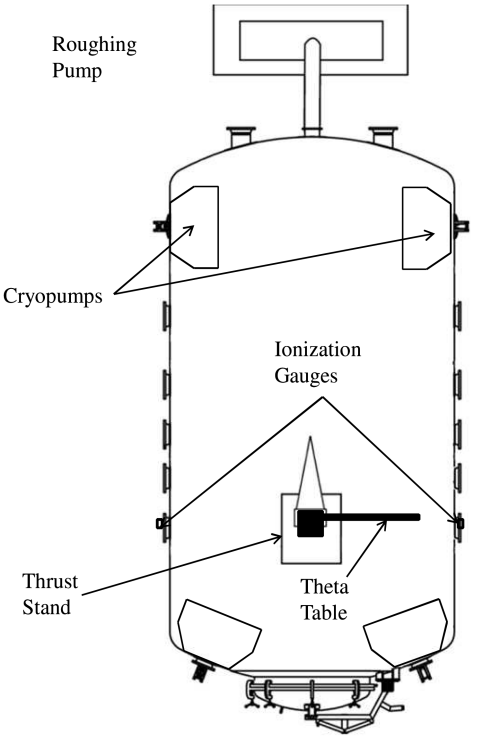

Fig. 4 Schematic of VTF-2 (not to scale).

Magnet settings remained constant through all tests to provide the field structure shown in Fig. 1. The choice of constant magnetic field is made to limit the variables in the system and maintain the field structure. Optimizing the magnetic field for minimum discharge current during testing causes the field to become asymmetric and unshields one electrode. The electrode current can be pushed from one electrode to the other in this fashion. However, a varying magnetic field would introduce complications to the analysis because the shielded and unshielded electrodes would behave differently.

The thruster is run through a 1 h conditioning cycle before data is taken. The cathode flow rate is kept constant at 1 mg/s for all tests. All three plume probes are placed 1 m downstream of the thruster exit plane on a radial motion arm centered above the exit plane. The probes are spaced 5 deg apart on the probe arm and individually aligned to thruster center with a laser tool.

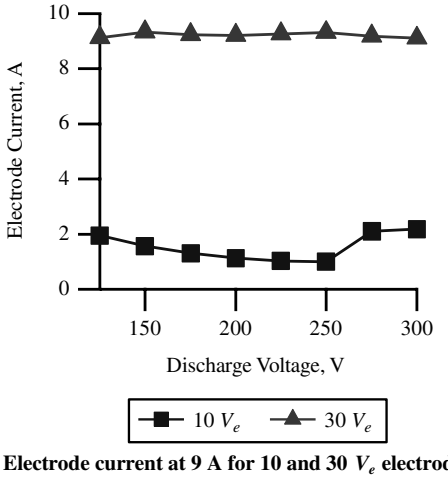

Fig. 5 Electrode current at 9 A for 10 and 30 V_e electrode bias.

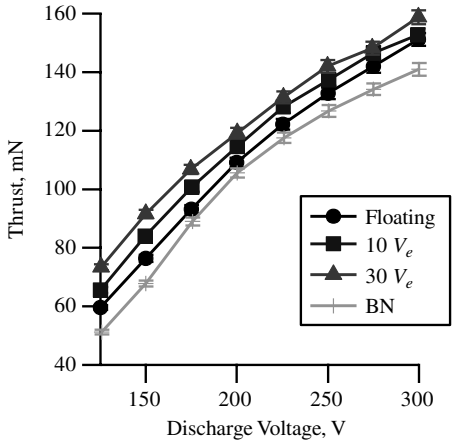

Fig. 6 Thrust at 9 A on xenon at floating, 10 V_e, and 30 V_e electrode bias and BN rings.

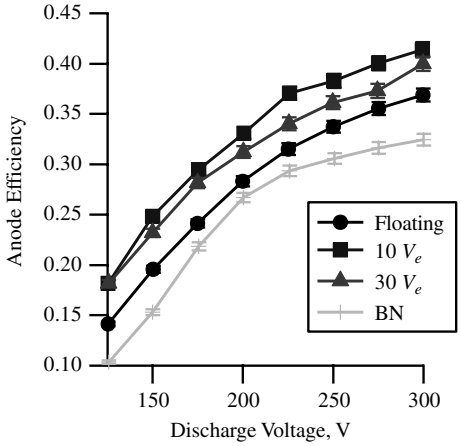

Fig. 9 Anode efficiency at 9 A on xenon at floating, 10 V_e, and 30 V_e electrode bias and BN rings.

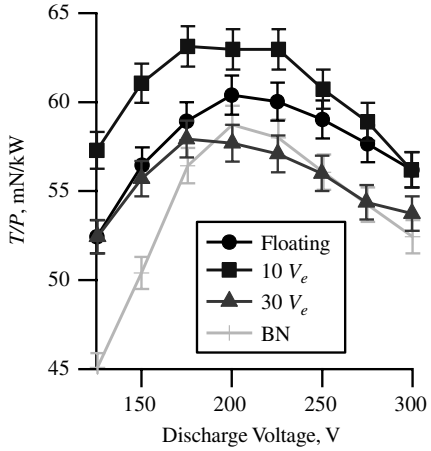

Fig. 7 T/P at 9 A on xenon at floating, 10 V_e, and 30 V_e electrode bias and BN rings.

A. Thrust Stand Results

Figures 6–9 show the performance (thrust, T/P ratio, I_{SP}, and anode efficiency) of the EEHET running on xenon at 9 A. Additionally, data for a no electrode configuration are shown. In this case, the graphite electrodes are replaced with boron nitride (BN) rings to approximate the original discharge channel. The data set is labeled as BN in the results. The T/P ratio, anode efficiency, and specific impulse calculations use the total mass flow rate and the total discharge power, which includes both anode and electrode powers as seen in Eqs. (1–3).

$$\frac{T}{P} = \frac{T}{P_d + P_e} = \frac{T}{P_{\text{tot}}} \tag{1}$$

$$n_A = \frac{1}{2}\frac{T^2}{\dot{m}_{\text{tot}} P_{\text{tot}}} \tag{2}$$

$$I_{\text{SP}} = \frac{T}{\dot{m}_{\text{tot}} g} \tag{3}$$

The thruster performance with BN rings on average is lower than the floating condition. The addition of the electrodes does appear to affect the thruster performance. This is attributed to the change in material from BN to graphite. Graphite has a lower secondary electron emission (SEE) that BN and thus contributes fewer cold electrons to the plasma. This can create a local zone of hot plasma that can provide increase ionization or acceleration potential.

The thruster performance increased along all four metrics with biased electrodes. T/P and efficiency are higher at 10 V_e than at 30 V_e. The 30 V_e case has larger increases in thrust than 10 V_e; however, there is a large increase in electrode power at 30 V_e, which reduces the T/P ratio and efficiency. At 30 V_e, the electrodes collect over 9 A of current. The current on the main anode is reduced to less than 1 A. The overall currently supplied by the discharge power supply is still kept at 9 A, however. This means there is some amount of current circulation between the electrodes and anode. The maximum total T/P ratio increase occurs at 150 V_d, resulting in a gain of 7.69 mN of thrust, 4.6 mN/kW thrust-to-power, 123 s I_{SP}, and 5.3% anode efficiency. Chamber operation pressure is between 5×10^{-6} and 7.7×10^{-6} Torr-Xe for all tests. The uncertainties estimated at $\pm 1.5\%$ for thrust and $\pm 3\%$ for all other metrics are included in the figure. The performance of the EEHET is lower or on par compared with the available data for the original T-220HT. A direct comparison between the two is not strictly valid because the EEHET has modified thruster magnetic field, magnetic flux pieces, and discharge channel.

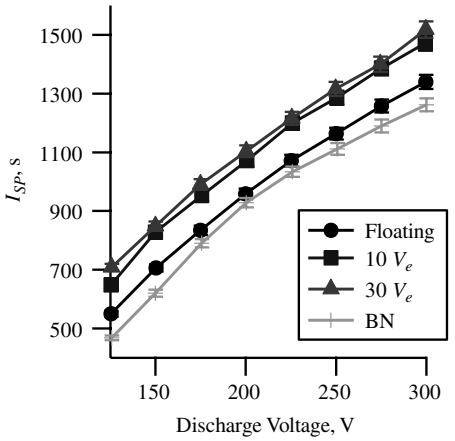

Fig. 8 Specific impulse at 9 A on xenon at floating, 10 V_e, and 30 V_e electrode bias and BN rings.

B. Faraday Probe Results

Plume measurements are taken at the same operation conditions as Figs. 6–9 minus the BN case, namely 125–300 V_d and 9 A discharge with floating, 10 V_e, and 30 V_e. Figure 10 shows the measured ion current density for the floating case from −100 to 100 deg at a few discharge settings to allow readability. The current density increases as the discharge voltage is increased as expected. Higher discharge voltage results in stronger electric fields and greater ionization and

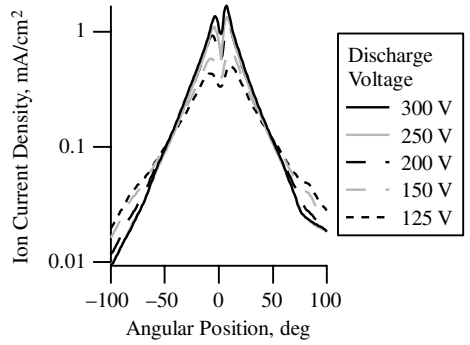

Fig. 10 Current density map for 125–300 V discharge with floating electrodes at 9 A.

thus larger ion current densities. The anode mass flow rate varies from 10.02 to 10.36 mg/s to maintain current as shown in Table A1 in the Appendix. The profile is not perfectly symmetrical. At large angles the left side exhibits lower current than the right. This is most likely due to some asymmetry in the thruster or alignment.

The EEHET exhibits a double peak structure that signifies that the focal length is longer than 1 m. The peaks rest between 6 and 9 deg on either side of the centerline. The current densities decrease with discharge voltage, and thus acceleration and ionization capability decreases, resulting in fewer ions. Thus lower voltages see an increase in electron current. All of the data are taken at nearly constant discharge currents as shown in Table A1 in the Appendix. Figure 11 shows the change in the current density with biased electrodes for 125 V_d. The 10 V_e case shows a minor change from the floating case, but 30 V_e creates a noticeable change in the current density. The current density increases at small angles resulting in larger peaks and decreases at large angles. The increase at small angles without a net upward shift of the entire plot is commonly attributed to collimated or

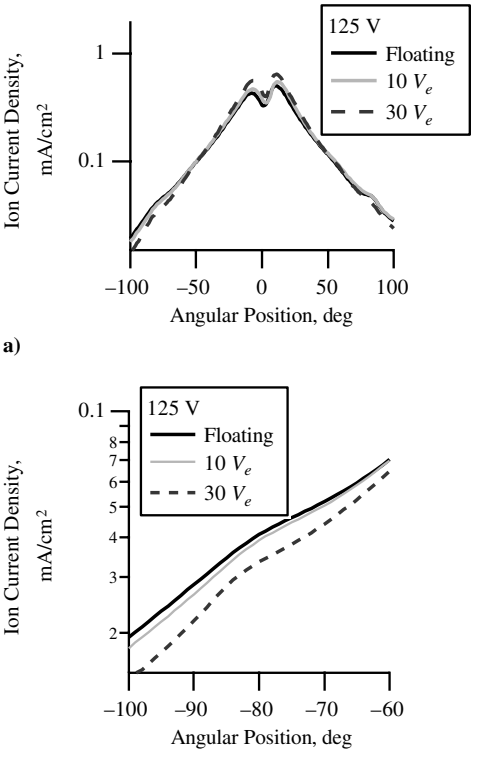

Fig. 11 Ion current density profile for 125 V_d, 8.93 A for floating, 10 V_e, and 30 V_e cases: a) entire profile and b) left side to show the decrease at large angles.

focused ion beam and reduced plume divergence. This is further supported by the decrease at large angles. The graph in Fig. 11b shows a magnified view of the same data at large angles. The effect is similar but smaller on the right side of the profile.

Figure 12 shows the current fractions for 10 and 30 V_e at different discharge voltages. The current fraction is the ion current density with biased electrodes normalized by their respective floating current densities. The graphs show more clearly the change in current density near centerline and at large angles. This effect is more evident at low V_d, which matches the observed performance improvements. At 300 V_d, the ion current density with electrodes actually drops below the floating data. The chamber pressure generally decreased or stayed constant with increased electrode bias; thus background charge-exchange collisions are not the cause of the changes.

At any given voltage, the discharge current is kept approximately constant about 9 A, and the magnet settings are also kept constant throughout the test. The only difference is the electrode power. As electrode bias increased, so did the current seen by the electrodes. The average electrode currents at 10 and 30 V_e are 1.5 and 9.2 A, respectively. The increase in the ion current density around centerline and decreases in the wings is attributed to a narrowing of the ion beam and decreased plume divergence angle. Figure 13 shows the plume divergence angle for all three cases (floating, 10 V_e, and 30 V_e). The ion current density is adjusted by using the linear extrapolation method to account for charge-exchange collisions at large angles [6]. A linear fit of the 10–30 deg data on a semi-log plot is extended to 90 deg. This method can underpredict the ion current density. The mathematical analysis to determine plume angle and beam current is performed with the method developed by Brown [12,15] to correct for the probe gap and the discrepancy between the discharge geometry and the point source measurement geometry. Faraday probe measurements have historically been marred by high degrees of uncertainty. Even recent work has claimed uncertainties up to ±50% [16]. Brown [5] recommended a thorough set of procedures for far-field Faraday probe measurements that can reduce the uncertainty to 5%. However, the full procedure was not performed for the data presented here. In an effort to provide a more consistent measurement of the uncertainty for plume angle, the two-way analysis of variance (ANOVA) was used [17]. The standard error from ANOVA is given by Eq. (4) for a 95% confidence interval. X and X_m are the actual and measured values, $t_{.95,\mathrm{dof}}$ is the value of the two-tailed t distribution, MS_E is the mean squares error, and r is the number of data repetitions. The resultant 95% confidence for the plume angle has a width of 4.8 deg, which gives a ±10% uncertainty.

$$X = X_m \pm t_{.95,\mathrm{dof}} \sqrt{\frac{MS_E}{r}} \tag{4}$$

The large uncertainty makes definite statements and conclusions about the plume divergence difficult; however, the trends suggest that the electrodes do decrease the plume divergence angle to a degree, primarily at low discharge voltages. The decrease is only noticeable below 150 V_d. Above that, the three cases have nearly identical plume angles, especially considering the uncertainty. Along with the increase in thrust observed, a decreased plume angle suggests either increased axial ion velocities or increased ion density.

C. RPA Results

Ion energy measurements are taken with the RPA at 10 angular positions around the plume. From 0 to 30 deg measurements are taken in 5 deg increments, and from 40 to 60 deg measurements are taken in 10 deg increments. One RPA sweep at each location is taken; however, three measurements at each ion repulsion grid potential are taken and averaged to produce the recorded value. A fourth order Savitzky–Golay smoothing filter is applied to the raw data prior to taking the derivative. Figure 14 shows the ion energy distribution function on thruster centerline for a few discharge settings with floating electrodes. The profile shows that the ion energy distribution function increases and broadens as the discharge voltage increases.

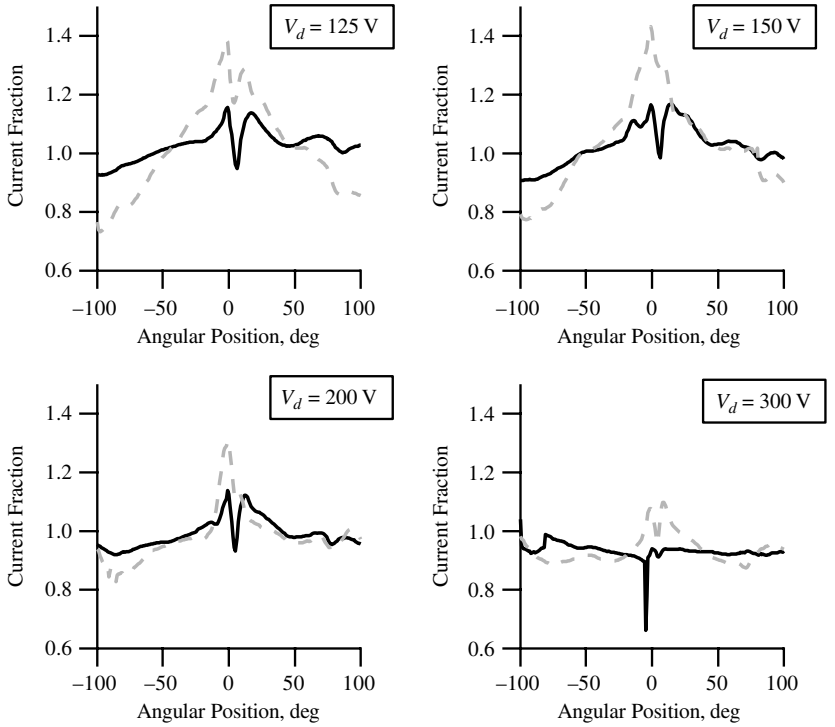

Fig. 12 Current fraction (ion current density normalized by the floating current density) showing 10 V_e/floating (solid line) and 30 V_e/floating (dotted line).

This is expected, because high voltages result in increased energy distribution and thus a larger spread in possible ion energies.

Figure 15 shows the computed ion energy distribution function when the thruster is operating at 175 V_d and 9 A for all three electrode cases at four angular locations. The biased electrodes cause a rightward shift in the ion energy distribution function, which results in increased ion energy. Similar trends are observed for other discharge voltages. At 10 V_e, there is a slight rightward shift of the ion energy distribution, on the order of a few volts. At 30 V_e, the shift is an average of 20 V. Figure 16 shows the centerline ion energy for all the conditions tested. The same trend in ion energy is observed at all discharge levels. Figure 17 plots the most probable ion energy for the 175 V_d operating conditions at all measured angles showing the effect occurs throughout the plume as well. There is a definite change in behavior from 10 V_e to 30 V_e that will be discussed later.

IV. Discussion

The goal of this work is to reduced ion-wall neutralization, thereby increasing the ion number density and decreasing plume divergence. Evidence that this has occurred would present as an increased ion current density for the same propellant and a more collimated ion beam. Evidence of a more collimated ion beam is a decrease in the plume divergence angle, an increase in ion density at small angles from thruster centerline, and a decrease in ion current density at large angles. As Fig. 13 shows, there is indeed a decrease in the plume divergence angle when the electrodes are biased above anode potential. This divergence angle decrease with electrodes is not unexpected. Previous work done with secondary electrodes in the discharge channel also showed a decreased plume divergence angle [18,19]. Although in those works the electrodes were placed near the channel exit, downstream of the radial magnetic field peak, no cusp fields were used. At 10 V_e, the plume divergence angle reduction is very minor. At 30 V_e, the angle decreases by up to 5 deg. The current density profiles increases around the centerline of the thruster and decreases at large angles as electrode bias is increased. The change is small at 10 V_e and larger at 30 V_e.

One important question is where the additional power from the electrodes is going. At 10 V_e, the electrodes increase total T/P, but at 30 V_e, the electrode decrease total T/P even though the thrust increase is higher at 30 V_e. These results suggest different power

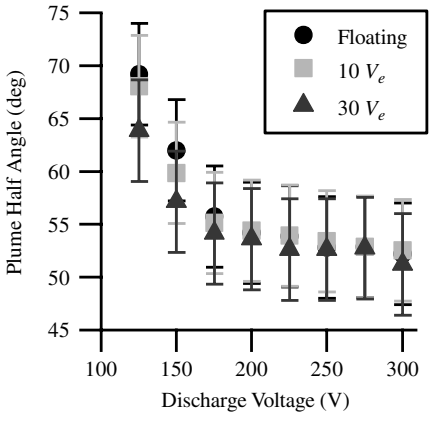

Fig. 13 Plume divergence half angle.

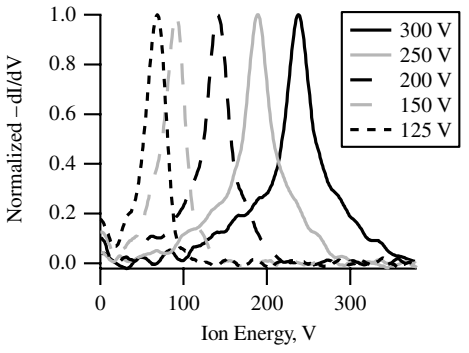

Fig. 14 Ion energy distribution function on thruster centerline for floating electrodes at 9 A.

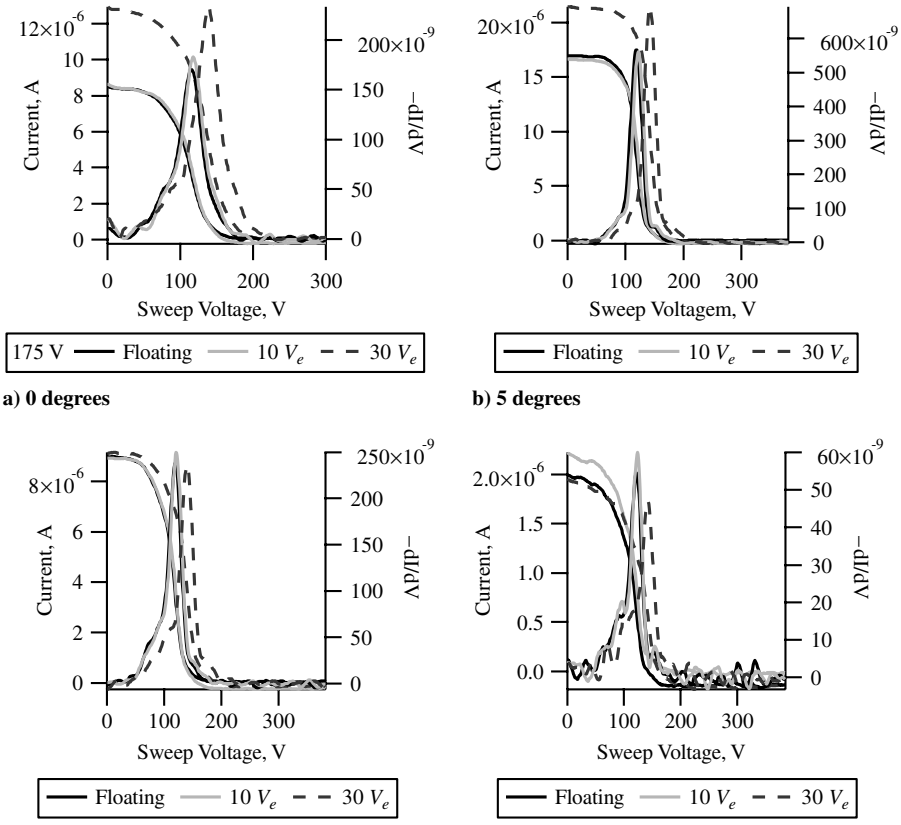

Fig. 15 Ion energy distribution function with electrodes at 175 V discharge voltage at various angles.

sinks for the electrodes at the two bias levels. The electrode power is likely coupled to the plasma to either accelerated ions, increases ion number, or is directly lost to Joule heating. Joule losses cannot be the sole energy sink because beneficial changes in thruster behavior are observed at 10 V_e. Figure 18 shows the change in most probable ion energy from floating to 10 V, and floating to 30 V_e at thruster centerline. At 10 V_e, there is very little contribution to ion acceleration from the electrodes except at low discharge voltages. Comparatively, at 30 V_e the electrodes provide over two-thirds of their added potential as acceleration. Again this increase in ion energy is greater at lower discharge voltages. In both electrode conditions, an increase in the propellant efficiency is observed. This translates to increased ion number density, which can be caused by increased ionization or ion focusing.

A. Ionization vs Ion Focusing

At this point, a discussion about ionization versus focusing is necessary. Figure 19 plots the propellant efficiency, which is defined simply as the measure beam current from the Faraday probe divided by the total mass flow rate. The thruster exhibits increased propellant efficiency with electrodes. The two ways to increase the ion number density are increased ionization, either by ionizing more neutrals or by increased ionization fraction, or reducing ion losses through focusing. The first method, increased neutral density resulting in increase ion density, is ruled out by virtue of constant or decreasing total mass flow with increased electrode bias. Figure 20 shows the total mass flow, anode plus cathode, for the floating, 10 V_e, and 30 V_e conditions tested. Table A1 in the Appendix lists the individual anode flow rates without the constant 1 mg/s cathode flow. With a

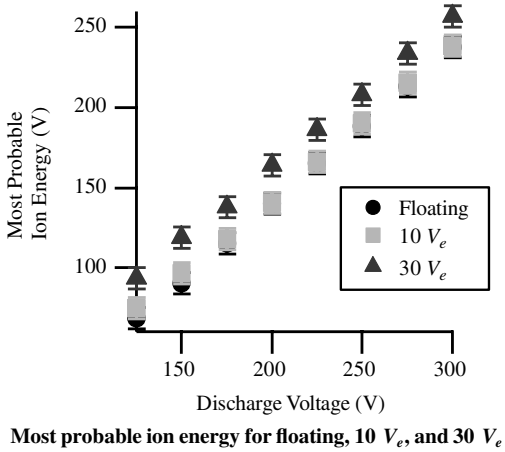

Fig. 16 Most probable ion energy for floating, 10 V_e, and 30 V_e at 9 A.

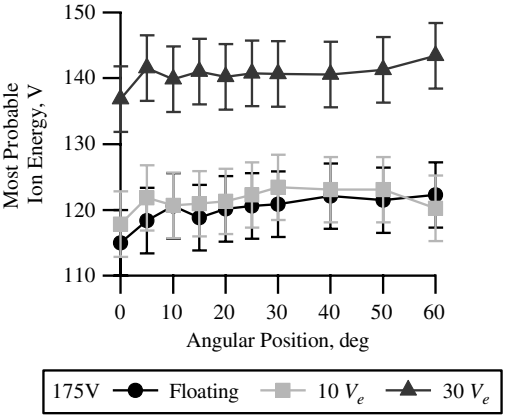

Fig. 17 Most probable ion energy for the ion energy distribution function at each measured angle on xenon at 175 V and floating (8.98 A discharge), 10 V_e (9.02 A), and 30 V_e (8.98 A).

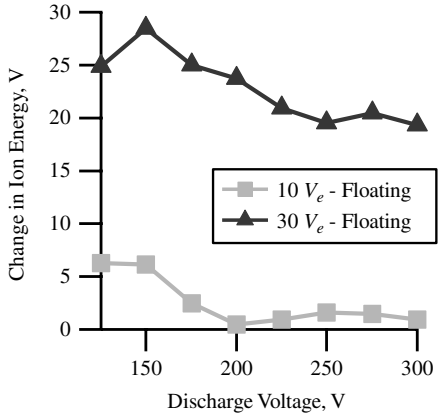

Fig. 18 Change in most probable ion energy from floating to 10 V_e and floating to 30 V_e at centerline.

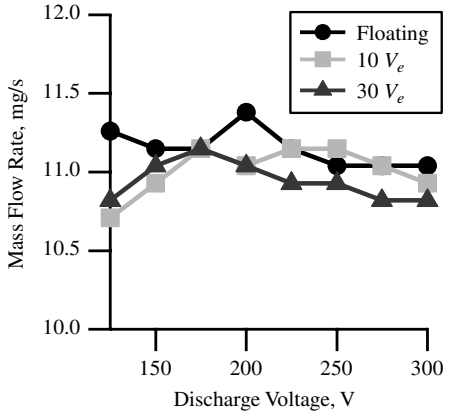

Fig. 20 Total mass flow rate including cathode flow. There is an overall decrease in mass flow rate with increased electrode bias.

few exceptions, to maintain constant discharge current, the mass flow rate decreased or remained constant with increased electrode bias. This means the ion number density increased without a corresponding increase in propellant neutrals. This rules out increased neutral density as a cause for the increased ion density.

The second method to increase ion density is increased ionization. Normally this effect is studied using an ExB probe to determine the ionization states and the ionization costs [20]. Unfortunately such data are not available. A rough analysis of the effect of ionization fraction can be done by comparing the change in propellant efficiency for floating versus the electrode cases. Figure 21 compares the change in propellant efficiency for the 25 V increases in discharge voltage in the floating case to the 10 and 30 V increases in electrode voltage for the electrode cases. For example, in the floating case, the change in propellant efficiency going from 125 to 150 V_d is 0.019, and the change from 150 to 175 V_d is 0.04. This graph shows that a 10 or 30 V increase in electrode potential caused a larger increase in propellant efficiency than a 25 V increase in anode potential. This result suggests that increasing the electrode potential by 10 or 30 V over the anode potential has effects other than increase ionization potential. There is a secondary effect causing the increased ion number density with biased electrode, which is suggested to be an ion-wall repulsion, or ion focusing, that increases ion number density by reducing the amount lost to neutralizations. This is more likely to be true for 10 V_e because improvements are seen in performance and propellant efficiency without large changes in ion energy. For the 30 V_e case, the electrodes collect almost all of the discharge current and become the dominant anode. This makes increased ionization rate a possible cause for the improvements and is discussed more in the next section.

B. Behavioral Differences with Electrodes

The ion energy distribution functions increases as the electrode bias increases. Figure 16 showed the most probable ion energy for the various test conditions. At 10 V_e, the increase in ion energy is small, a maximum of 6.3 V for the 125 V_d case. At 30 V_e, the increase ranges from 19 to 25 V. Although the increase in ion energy is small at 10 V_e, there is a significant increase in thrust and T/P ratio over the floating case (up to 7.69 mN and 4.6 mN/kW improvement). At 30 V_e, the thrust increases even more (up to 13.7 mN); however, the electrodes also see a marked increase in collected current, which leads to a reduction in the T/P ratio (loss of 1–3 mN/kW).

Looking back at Fig. 18, the different level of ion energy increase between 10 and 30 V_e suggests that the electrodes function differently at the two bias levels. At 30 V_e, the majority of their power goes into ion acceleration, increasing the potential fall experienced by the ions. At 10 V_e, the power of the electrode is channeled into another aspect of the plasma, presumably ion-wall repulsion. Additionally, the increase in ion energy is larger at low discharge voltages. The differences between low and high discharge voltages can simply be due to the electrode potential relative to discharge potential. At 125 V_d, 10 V is a larger fraction of the total potential than at 300 V_d. So a 10 or 30 V_e increase will have a greater effect lower energy ions. At lower discharge voltages, a larger fraction of the discharge energy is applied to ionization with less Joule losses than at high voltages [20]. This means the s mall voltage addition of the electrodes will likely have a more visible effect at lower discharge voltages where it is less likely to be lost to heating.

The behavioral difference between 10 and 30 V_e is most likely cause by the changing electrode currents. Figure 5 showed the

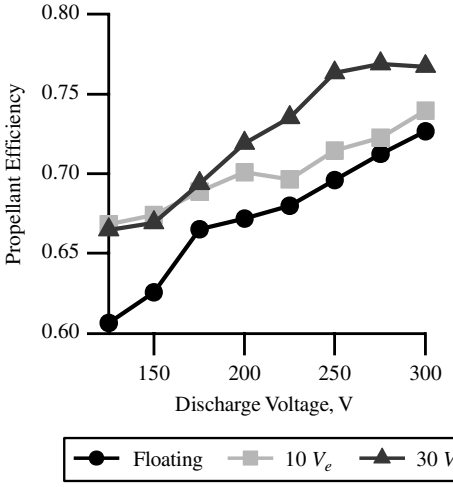

Fig. 19 Propellant efficiency defined as beam current/total mass flow rate.

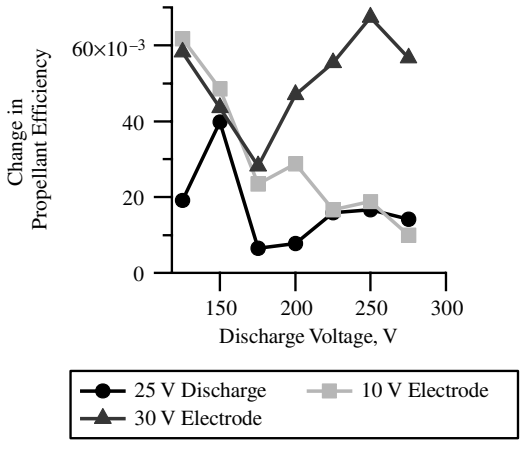

Fig. 21 Change in propellant efficiency comparing 25 V discharge increase from floating to 10 and 30 V_e electrode increases.

collected current as a function of the discharge voltage. At 10 V_e, the electrodes collect less than 2.17 A of current. The electrodes are electrically connected to the main anode; thus there is current sharing. The main discharge power supply is kept at 9 A, and it supplies both the electrode and anode currents. Thus any current to the electrodes reduces current to the anode. At 30 V_e, the electrodes collect over 9 A of current, surpassing the discharge power supply. The extra collected current must come from a recycled current between the electrodes and anode. At 30 V_e, the electrodes become the primary anode and dictate the plasma behavior. This is seen in the ion energy measured by the RPA. Figure 16 showed that at a given discharge voltage, the 30 V_e measurement approximately matches the floating measurement for the next higher discharge voltage (200 V, 30 $V_e \approx 225$ V). Kieckhafer [19] showed in a similar experiment that the thruster responds to the highest voltage in the circuit. In that work, when the electrodes collect all of the current and are above the anode voltage, the ion energy increased in response. A similar ion energy increase is seen at 30 V_e. This in turn causes an increase in the maximum "discharge" potential in the channel. The increase of maximum potential could explain some of the observed changes at 30 V_e such as increased thrust.

The comparison of propellant efficiency in the previous section seems to indicate a 30 V_e increase does not have the same effect as a similar increase in discharge voltage. A second possible cause of the increased propellant efficiency is increased ionization caused by increased neutral residence time. By pulling current from the anode, the anode temperature decreases. In turn, the lower temperature reduces the propellant thermal velocity and can cause increased ionization and beam current [21]. Massey et al. [22] showed that a 50°C decrease in anode temperature is possible with a ~4.5 A decrease in anode temperature. At 30 V_e, there is a shift of ~9 A of current from the anode, which can result in a large temperature drop. However, in all previous experiments with anode cooling, small increases in performance or negative performance changes were seen [19,21,23]. The results of this work show noticeable performance gains beyond the error at both electrode bias levels. An increased neutral residence time may play some small part in the increase in propellant efficiency but is likely not the direct cause.

The primary difference between the electrode and propellant distributor acting as the main anode is the location. Material considerations likely play a small part because both graphite and molybdenum are conducting materials with low SEE values. The electrodes are located further downstream and closer to the channel exit. This may cause the potential field within the thruster to change when the dominant high voltage source location is changed. Ions and electrons may also be collected downstream of the anode by the electrodes and thus create a dearth near the anode.

A possible explanation of the difference from floating to 10 V_e and then to 30 V_e is expansion of the plasma sheath. At 10 V_e, the plasma sheath surrounding the electrode shields out the electric field from the majority of the plasma. The electrode thus only affects a small fraction of the plasma. Once the electrodes increase to 30 V_e, the near-wall plasma sheath may grow to compensate for the increased potential. This allows the electric field to reach out further and affect a larger portion of the bulk plasma. Anders [24] shows with a DC-biased flat substrate that the sheath thickness does increases with surface bias. In that work, however, the substrate is biased to many kilovolts of potential, and the sheath thickness increase is on a few millimeters, but the relation is likely still valid at lower voltages.

Another contribution to sheath thickness could be the near-wall magnetic fields. The static magnetic field in Fig. 1 shows cusp fields surrounding the two electrodes. The intent of these fields is to reduce electron collection. A secondary effect of oblique or parallel fields near a surface is the extension and enlargement of the near-wall sheath. Research shows that magnetic fields next to wall surfaces can increase the thickness of the plasma sheath [25–28]. In the probe data presented, the magnets are kept constant and thus the magnetic field effects on the sheath can be assumed the same between 10 and 30 V_e. A preliminary test of the thruster with different ring cusp magnet settings does show a change in electrode current with magnet settings. Figure 22 shows the electrode current measured at 10 V_e as the shielding ring-cusp magnet currents are increased. The electrode current decreases at first in response to increased field strength around the electrodes that decrease electron transport; however, it rises slightly when the magnets are brought up to 15 A. This behavior indicates a secondary phenomenon occurring at a some magnetic field strength threshold in addition to trapping of electrons on field lines. The two effects of a biased surface and near-wall cusp magnetic field could in part explain the changes seen in ion energy. In-channel measurements of the near-wall plasma are necessary to further pursue this line of analysis.

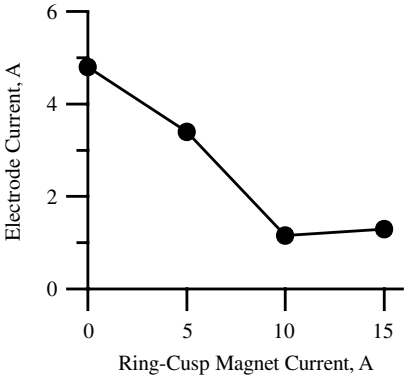

Fig. 22 Electrode current as function of ring-cusp shielding magnet currents at 175 V, 9 A discharge, and 10 V_e.

V. Conclusions

This work showed that the addition of focusing electrodes in the discharge channel has positive effects on Hall thruster performance. A modified T-220HT Hall thruster, dubbed the embedded electrode Hall-effect thruster, is tested on xenon at 9 A at several combinations of discharge voltage and electrode bias voltage. The electrodes cause a definite increase in thruster performance across all four metrics of thrust, total T/P ratio, anode efficiency, and specific impulse at 10 V electrode bias. The 30 V electrode setting increased thrust but causes the T/P ratio to decrease because of a jump in electrode current. Plume measurements show an increased current density near the centerline and a decrease at large angles. Along with increased ion beam current, this points to increased ion number density, specifically near the centerline of the thruster. The goal of this work is to reduce ion-wall neutralizations with wall electrodes to collimate ions. This seems to have been accomplished.

The Retarding Potential Analyzer data show increased average ion energy. The increase is small at 10 V_e and much larger at 30 V_e. Because the discharge conditions did not change, this means the electrodes provided an additional acceleration to the ions in addition to any ion focusing. The increased ion number density with constant or decreasing mass flow means an increased propellant efficiency with electrode bias. The increase in propellant efficiency cannot solely be explained with increased ionization rate, thus giving evidence of ion focusing. The difference in level of ion energy change between the two electrode conditions suggests that the thruster is operating in two different modes, dependent on electrode bias. The biased electrode may extend the near-wall plasma sheath thickness as seen by other researchers. An increased plasma sheath caused by near-wall cusp magnetic fields may also have a part in the observed differences, but the plume plasma response to a changing magnetic field data was not taken here. The physics in a Hall-effect thruster are complex, and more may be occurring here than can be inferred from the data presented here. Further study of the plume and in-channel discharge plasma and numerical modeling is required to better understand the observed behaviors.

Appendix: Operating Conditions

Table A1 Operating conditions for the data presented

Discharge voltage	Electrode voltage	V_{CG}, V	Anode mass flow, mg/s[a]	I_d, A	I_e, A	Thrust, mN	T/P, mN/kW	I_{SP}, s	η_A	P_c, Torr-Xe
300	BN	−17.4	9.88	8.97	0	141.1	52.44	1263	0.325	5.82E − 6
275	BN	−17.4	9.99	9.00	0	134.3	54.23	1190	0.317	6.08E − 6
250	BN	−16.9	10.10	9.02	0	126.7	56.07	1113	0.306	6.70E − 6
225	BN	−16.4	10.10	8.98	0	117.7	58.01	1033	0.294	6.70E − 6
200	BN	−16	10.10	8.98	0	105.6	58.74	927	0.267	6.70E − 6
175	BN	−15.3	10.00	8.98	0	89.0	56.42	789	0.218	6.10E − 6
150	BN	−14.6	9.66	8.98	0	67.9	50.40	620	0.153	5.02E − 6
125	BN	−13.8	9.66	9.05	0	51.3	45.09	468	0.104	5.02E − 6
300	Floating	−22.7	10.02	9.12	0	151.1	56.19	1339	0.369	5.93E − 6
275	Floating	−22.5	10.02	9.03	0	142.0	57.66	1258	0.356	5.93E − 6
250	Floating	−21.9	10.02	8.97	0	132.8	59.05	1165	0.337	5.93E − 6
225	Floating	−21.3	10.14	8.92	0	122.2	60.04	1071	0.315	6.28E − 6
200	Floating	−20.5	10.36	8.93	0	109.2	60.39	957	0.283	7.70E − 6
175	Floating	−19	10.36	8.98	0	93.2	58.95	834	0.241	7.70E − 6
150	Floating	−18.7	10.14	8.90	0	76.3	56.48	705	0.195	6.28E − 6
125	Floating	−16.3	10.25	8.93	0	59.5	52.45	550	0.142	7.10E − 6
300	10 V	−22.4	9.91	9.00	2.17	152.7	56.20	1473	0.414	5.93E − 6
275	10 V	−22.3	10.02	8.97	2.11	146.6	58.91	1386	0.400	5.93E − 6
250	10 V	−21.9	10.02	9.10	1.0	142.0	62.74	1329	0.409	5.58E − 6
225	10 V	−21.1	10.14	9.00	1.03	128.3	62.97	1200	0.371	6.28E − 6
200	10 V	−20	10.36	9.02	1.13	114.5	62.97	1072	0.331	7.70E − 6
175	10 V	−19.4	10.25	9.02	1.3	100.8	63.15	953	0.295	7.60E − 6
150	10 V	−18.7	9.91	9.08	1.56	83.99	61.08	828	0.248	5.93E − 6
125	10 V	−16.8	9.80	9.00	1.94	65.7	57.29	647	0.182	5.23E − 6
300	30 V	−21.5	9.80	8.98	9.1	158.8	53.74	1517	0.400	5.23E − 6
275	30 V	−21.5	9.80	8.97	9.18	148.1	54.36	1400	0.373	5.23E − 6
250	30 V	−21.5	9.91	9.03	9.32	142.0	56.00	1316	0.361	5.93E − 6
225	30 V	−21.2	9.91	8.98	9.25	131.3	57.09	1217	0.341	5.93E − 6
200	30 V	−20.9	10.02	8.90	9.21	119.1	57.71	1103	0.312	5.58E − 6
175	30 V	−20.1	10.14	8.98	9.23	106.9	57.94	990	0.281	6.28E − 6
150	30 V	−19	9.91	8.93	9.34	91.6	55.69	849	0.232	5.93E − 6
125	30 V	−17.8	9.80	8.90	9.12	73.3	52.44	707	0.182	5.23E − 6

[a]Mass flow does not include cathode flow rate of 1 mg/s.

Acknowledgments

The research contained herein is sponsored by American Pacific In-Space Propulsion. Kunning Xu is supported by the National Defense and Science Engineering Graduate Fellowship and the Georgia Tech Institute Fellowship. The authors are greatly appreciative of this support. We would like to thank Pratt & Whitney for supplying HPEPL with the T-220HT, Gregory McCormick for work in simulation and modifications, Hoang Dao for programming assistance, and departmental technical staff and other graduate students at HPEPL for assistance with this work.

References

[1] Morozov, A. I., Esipchuk, Y. V., Tilinin, G. N., Trofimov, A. V., Sharov, Y. A., and Shchepkin, G. Y., "Plasma Accelerator with Closed Electron Drift and Extended Acceleration Zone," *Soviet Physics: Technical Physics*, Vol. 17, No. 1, 1972, pp. 38–45.

[2] Hofer, R. R., "Development and Characterization of High-Efficiency, High-Specific Impulse Xenon Hall Thrusters," Aerospace Engineering, Ph.D. Dissertation, Univ. of Michigan, Ann Arbor, MI, 2004.

[3] Pote, B., and Tedrake, R., "Performance of a High Specific Impulse Hall Thruster," *27th International Electric Prouplsion Conference*, IEPC Paper 01-35, Pasadena, CA, 2001.

[4] de Grys, K., Rayburn, C., Wilson, F., Fisher, J., Werthman, L., and Khayms, V., "Multi-Mode 4.5 kW BPT-4000 Hall Thruster Qualification Status," *39th AIAA Joint Propulsion Conference*, AIAA Paper 2003-4554, Huntsville, AL, 2003.

[5] Brown, D. L., "Investigation of Low Discharge Voltage Hall Thruster Characteristics and Evaluation of Loss Mechanism," Aerospace Engineering, Ph.D. Dissertation, Univ. of Michigan, Ann Arbor, MI, 2009.

[6] McVey, J. B., Britt, E. J., Engelman, S. F., Gulczinski, F. S., Beiting, E. J., and Pollard, J. E., "Characteristics of the T-220HT Hall-Effect Thruster," *39th Joint Propulsion Conference*, AIAA Paper 2003-5158, Huntsville, AL, 2003.

[7] Xu, K. G., and Walker, M. L. R., "High-Power, Null-Type, Inverted Pendulum Thrust Stand," *Review of Scientific Instruments*, Vol. 80, 2009, Paper 055103. doi:10.1063/1.3125626

[8] Manzella, D. H., and Sankovic, J. M., "Hall Thrusters Ion Beam Characterization," *31th AIAA Joint Propulsion Conference*, AIAA Paper 95-2927, San Diego, CA, 1995.

[9] Walker, M. L. R., Hofer, R. R., and Gallimore, A. D., "The Effects of Nude Faraday Probe Design and Vacuum Facility Backpressure on the Measured Ion Current Density Profile of Hall Thruster Plumes," *38th AIAA Joint Propulsion Conference*, AIAA Paper 2002-4253, Indianapolis, IN, 2002.

[10] Hofer, R. R., Walker, M. L. R., and Gallimore, A. D., "A Comparison of Nude and Collimated Faraday Probes for Use with Hall Thrusters," *27th International Electric Propulsion Conference*, IEPC Paper 01-020, Pasadena, CA, 2001.

[11] Mason, L. S., and Jankovsky, R. S., "1000 Hour of Testing on a 10 Kilowatt Hall Effect Thruster," *37th AIAA Joint Propulsion Conference*, AIAA Paper 2001-3773, Salt Lake City, UT, 2001.

[12] Brown, D. L., and Gallimore, A. D., "Evaulation of Facility Effects on Ion Migration in a Hall Thruster Plume," *Journal of Propulsion and Power*, Vol. 27, No. 3, 2011, pp. 573–585. doi:10.2514/1.B34068

[13] King, L. B., "Transport-Property and Mass Spectral Measurements in the Plasma Exhaust Plume of a Hall-Effect Space Propulsion System," Aerospace Engineering, Ph.D. Dissertation, Univ. of Michigan, Ann Arbor, MI, 1998.

[14] Hutchinson, I. H., *Principles of Plasma Diagnostics*, Cambridge Univ. Press, Cambridge, 1987.

[15] Brown, D. L., and Gallimore, A., "Evaluation of Ion Collection Area in Faraday Probes," *Review of Scientific Instruments*, Vol. 81, 2010, Paper 063504. doi:10.1063/1.3449541

[16] Reid, B. M., "The Influence of Neutral Flow Rate in the Operation of

Hall Thrusters," Aerospace Engineering, Ph.D. Dissertation, Univ. of Michigan, Ann Arbor, MI, 2009.
[17] NIST/SEMATECH e-Handbook of Statistical Methods, http://www.itl.nist.gov/div898/handbook.
[18] Raitses, Y., Dorf, L. A., Litvak, A. A., and Fisch, N. J., "Plume Reduction in Segmented Electrode Hall Thruster," *Journal of Applied Physics*, Vol. 88, No. 3, 2000, pp. 1263–1270. doi:10.1063/1.373813
[19] Kieckhafer, A. W., "The Effect of Segmented Anodes on the Performance and Plume of a Hall Thruster," Mechanical Engineering, Ph.D. Dissertation, Michigan Technological Univ., Houghton, MI, 2007.
[20] Brown, D. L., Larson, W., and Beal, B. E., "Methodology and Historical Perspective of a Hall Thruster Efficiency Analysis," *Journal of Propulsion and Power*, Vol. 25, No. 6, 2009, pp. 1163–1177. doi:10.2514/1.38092
[21] Book, C. F., and Walker, M. L. R., "Effect of Anode Temperature on Hall Thruster Performance," *Journal of Propulsion and Power*, Vol. 26, No. 5, 2010, pp. 1036–1044. doi:10.2514/1.48028
[22] Massey, D., Kieckhafer, A. W., Sommerville, J., and King, L. B., "Development of a Vaporizing Liquid Bismuth Anode for Hall Thrusters," *40th AIAA Joint Propulsion Conference*, AIAA Paper 2004-3768, Fort Lauderdale, FL, 2004.
[23] Peterson, P. Y., Massey, D., Shabshelowitz, A., Shastry, R., and Liang, R., "Performance and Plume Characterization of a Helicon Hall Thruster," *32nd International Electric Propulsion Conference*, IEPC Paper 2011-269, Wiesbaden, Germany, 2011.
[24] Anders, A., "Width, Structure and Stability of Sheaths in Metal Plasma Immersion Ion Implantation and Deposition: Measurements and Analytical Considerations," *Surface and Coatings Technology*, Vol. 136, 2001, pp. 85–92. doi:10.1016/S0257-8972(00)01017-3
[25] Cohen, R. H., and Ryutov, D. D., "Plasma Sheath in a Tilted Magnetic Field: Closing of the Diamagnetic Currents: Effect on Plasma Convection," *Physics of Plasmas*, Vol. 2, No. 6, 1995, pp. 2011–2019. doi:10.1063/1.871288
[26] DeWald, A. B., Bailey, A. W., and Brooks, J. N., "Trajectories of Charged Particles Traversing a Plasma Sheath in an Oblique Magnetic Field," *Physics of Fluids*, Vol. 30, No. 1, 1987, pp. 267–269. doi:10.1063/1.866185
[27] Anders, A., Anders, S., and Brown, I. G., "Effect of Duct Bias on Transport of Vacuum Arc Plasmas Through Curved Magnetic Filters," *Journal of Applied Physics*, Vol. 75, No. 10, 1994, pp. 4900–4905. doi:10.1063/1.355777
[28] Keidar, M., and Beilis, I. I., "Plasma-Wall Sheath in a Positive Biased Duct of the Vacuum Arc Magnetic Macroparticle Filter," *Applied Physics Letters*, Vol. 73, No. 3, 1998, pp. 306–308. doi:10.1063/1.121817

L. King
Associate Editor